Lab on a Chip

PAPER

Cite this: *Lab Chip*, 2015, **15**, 1942

Planar microfluidic drop splitting and merging

Sean Collignon, James Friend and Leslie Yeo*

Received 11th December 2014,
Accepted 24th February 2015

DOI: 10.1039/c4lc01453g

www.rsc.org/loc

Open droplet microfluidic platforms offer attractive alternatives to closed microchannel devices, including lower fabrication cost and complexity, significantly smaller sample and reagent volumes, reduced surface contact and adsorption, as well as drop scalability, reconfigurability, and individual addressability. For these platforms to be effective, however, they require efficient schemes for planar drop transport and manipulation. While there are many methods that have been reported for drop transport, it is far more difficult to carry out other drop operations such as dispensing, merging and splitting. In this work, we introduce a novel alternative to merge and, more crucially, split drops using laterally-offset modulated surface acoustic waves (SAWs). The energy delivery into the drop is divided into two components: a small modulation amplitude excitation to initiate weak rotational flow within the drop followed by a short burst in energy to induce it to stretch. Upon removal of the SAW energy, capillary forces at the center of the elongated drop cause the liquid in this capillary bridge region to drain towards both ends of the drop, resulting in its collapse and therefore the splitting of the drop. This however occurs only below a critical Ohnesorge number, which is a balance between the viscous forces that retard the drainage and the sufficiently large capillary forces that cause the liquid bridge to pinch. We show the possibility of reliably splitting drops into two equal sized droplets with an average deviation in their volumes of only around 4% and no greater than 10%, which is comparable to the 7% and below splitting deviation obtained with electrowetting drop splitting techniques. In addition, we also show that it is possible to split the drop asymmetrically to controllably and reliably produce droplets of different volumes. Such potential as well as the flexibility in tuning the device to operate on drops of different sizes without requiring electrode reconfiguration, *i.e.*, the use of different devices, as is required in electrowetting—therefore makes the present method an attractive alternative to electrowetting schemes.

1. Introduction

Open platforms in which discrete sessile drops are transported and manipulated on a two-dimensional planar substrate offer an attractive alternative to their conventional continuous flow one-dimensional closed microchannel counterpart. Not only are individual drops useful as compartmentalized carriers or reactors isolated from the surrounding matrix, these open drop microfluidic platforms also offer scalability, reconfigurability, and individual addressability of unit operations on a chip-scale device in a manner similar to traditional benchtop chemical or biochemical processes.[1–3] In addition to the requirement of substantially lower nanoliter to picoliter volumes—an important consideration when costly samples and reagents are employed, open drop platforms also reduce interfacial contact with surfaces, thus minimizing undesirable surface adsorption, which is a typical problem arising from electrostatic interactions in systems involving biomolecules,[4] and surface contamination of samples. Besides enabling a wide range of platforms for point-of-care medical diagnostics,[5,6] the ability to transport and manipulate drops on such platforms also finds useful applications in display technology and optics, among others.[7,8]

Central to these open microfluidic platforms is the ability to rapidly and precisely transport and manipulate individual sessile drops on a substrate, although at the expense of overcoming the resistive forces associated with viscosity, contact line pinning and surface energy.[9] Among these fundamental manipulations on planar substrates are drop dispensing (or creation), transport (or actuation), merging (or coalescence), and splitting (or cutting),[10] although drop dispensing and splitting appear to be the most complicated given the energy cost, *i.e.*, the surface free energy, associated with the disruption of intermolecular bonds and the subsequent creation of surface area during these operations.

One way to carry out such drop surgical operations is to alter its surface free energy by manipulating its wettability. This can be done, for example, by chemically or physically modifying the substrate with patterns of opposing hydrophilic (expansion) and hydrophobic (contraction) regions adjacent to each other or by translating a drop into hydrophobic obstacles

Micro/Nanophysics Research Laboratory, RMIT University, Melbourne, VIC 3000, Australia. E-mail: leslie.yeo@rmit.edu.au

to subsequently break them apart.[11] The necessity for such patterning however, limits the mobility of the post-split droplets. A more versatile and commonly used method is to employ electric fields to alter the wettability of a drop on a hydrophobic substrate.[12,13] In static electrowetting (in contrast to spontaneous electrowetting in which an electric field in the vicinity of the contact line generates a macroscopic Maxwell pressure gradient to drive bulk flow in the form of an advancing film front),[14] the near-singular electric field that arises upon application of a voltage across the drop produces a point Maxwell force that balances the surface forces at the contact line, giving rise to a change in the drop's contact angle dictated by the Lippmann condition.[15,16] As the drop merely relaxes under the applied Maxwell stress to its new equilibrium contact angle condition (*i.e.*, no bulk flow into the contact line region arises), which, by judicious design, causes it to overlap an adjacent electrode, it is then necessary to employ, and sequentially activate and deactivate, a series of individually controlled adjacent electrodes to cause the drop to march discretely along the electrode array sequence.[17] A sequential control logic scheme for the electrode activation/deactivation can then be programmed to carry out more sophisticated tasks such as drop dispensing, splitting and recombination.[10] For example, drop splitting can be achieved by activating the two electrodes that flank the electrode on which the drop rests in order to stretch it across the three electrodes, followed by deactivation of the center electrode to induce necking and subsequent pinching of the parent drop into two equal daughter droplets. Given such digitated motion, these electrowetting schemes have therefore been commonly referred to as digital microfluidics.[3]

While an extremely powerful and versatile tool for precise two-dimensional drop transport and manipulation on planar chip devices, electrowetting has a number of drawbacks. Most notably, the drop dimension and hence its volume is constrained by the size of the electrodes, given the necessity for the drop to span two adjacent electrodes at any one time in order to facilitate its relaxation to the adjacent electrode.[17] Therefore, variation in drop volumes post-fabrication of the device become problematic due to set electrode configurations, requiring new electrode designs and hence additional arrays or new devices. Other limiting factors for drop splitting include contact angle saturation, the height between the base and top electrodes in sandwich configurations, the time sequence for voltage activation, and the interfacial tension.[18]

In the present work, we propose an alternative method for planar drop splitting and recombination based on surface acoustic waves (SAWs),[19,20] which are nanometer amplitude Rayleigh-type electromechanical waves that are generated and that propagate on piezoelectric substrates. The ability of the SAW to transport sessile drops has been well documented,[21–28] enabled by the diffraction of sound waves into the drop at an angle known as the Rayleigh angle $\theta_R \approx \sin^{-1} c_l/c_{SAW}$ as a result of the mismatch of sound velocities within the substrate and drop, c_{SAW} and c_l, respectively. Attenuation of SAW energy at the Rayleigh angle gives rise to acoustic streaming in the drop contributing to a horizontal body force component that causes the drop to move in the direction of the SAW propagation if the force sufficiently overcomes the contact line pinning force (Fig. 1). Beyond these simple drop manipulations, in addition to mixing[29–31] and drop merging,[32,33] the ability to perform more complex drop operations such as splitting using SAWs in a precise, controllable and reproducible manner have yet to be reported. The splitting achieved in previous attempts by inertially jetting and hence ejecting part of a sessile parent drop to form a displaced daughter droplet, both using SAWs[34] and Lamb waves on superstrates,[35] for example, is difficult to control and is far from precise and reproducible. Where SAWs were combined with electrowetting for drop manipulation,[36] the acoustic field was primarily employed to merely translate the sessile drop to electrodes patterned on the chip where the electric field is able to modify the contact angle and hence split the drop.

2. Methodology

To split a drop, a pair of opposing body forces are required to elongate it to the point beyond which it cannot be restored by capillary pressure, such that the drop necks and pinches into two daughter droplets. However, it is not possible to achieve this simply using a pair of equally opposing SAWs as their overlap results in a standing wave, which results in a portion of the drop being trapped. As such, we employ a pair of SAWs laterally offset with respect to the position of the parent drop so that both exist flush against the other by using the electrode configuration shown in Fig. 2; similar offset IDTs have been used previously to drive azimuthal recirculation and hence microcentrifugation within the drop.[29,37] The drop is therefore subject to irradiation from both sides; the electrodes—1 μm thick aluminium interdigital

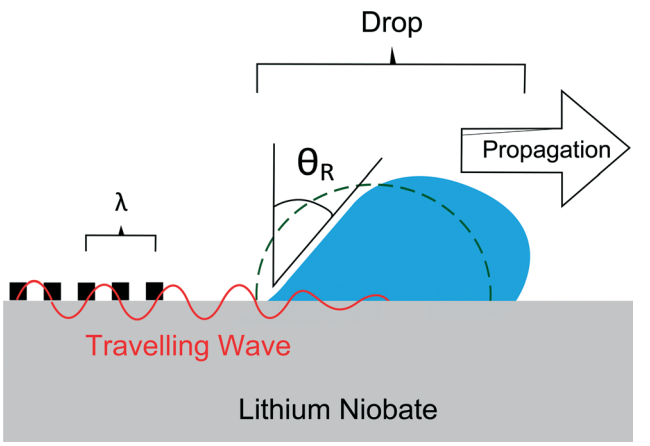

Fig. 1 Leakage of the SAW energy from the substrate into the liquid drop at the Rayleigh angle θ_R drives acoustic streaming within the drop, imparting a horizontal body force component that causes it to translate in the direction of the SAW propagation. Here the original sessile drop outline is represented by the dotted line.

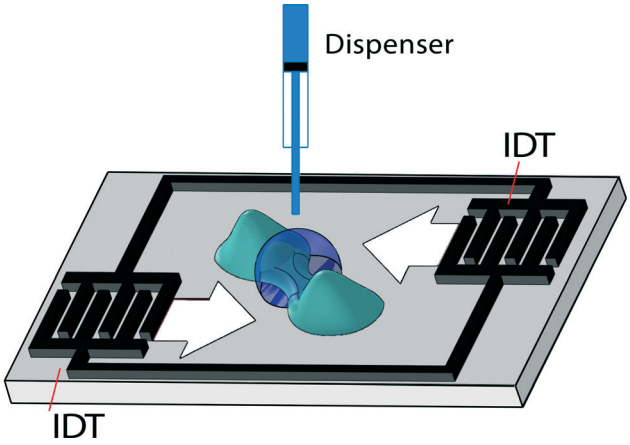

Fig. 2 Schematic illustration showing the laterally-offset interconnected IDT design for drop splitting using a pair of opposing SAWs, as indicated by the arrows. The device dimension is 17 mm × 24 mm and its thickness is 0.5 mm.

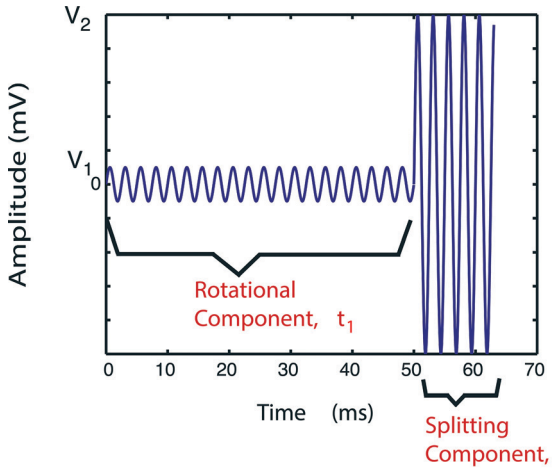

Fig. 3 Typical SAW energy input scheme for optimal drop splitting in which a 20 MHz SAW sinusoidal wave is amplitude modulated by a two-part step-up carrier wave (figure not to scale). The first phase comprises a rotational component which has a low carrier wave amplitude over a period t_1, which provides the initial energy as a precursor for stretching the drop whilst suppressing any propensity for it to jet. The second, splitting component consists of a sharp ramp up voltage in the carrier wave amplitude over a much shorter duration t_2 comparable to the inertial time scale to rapidly elongate the drop. Thus, the energies of these two components are labelled as the rotational energy E_R and the splitting energy E_S, respectively.

transducer (IDT) structures with aperture widths of 3 mm were patterned using standard photolithography and wet etch techniques onto 0.5 mm thick 128° *Y–X* single crystal lithium niobate substrate (Roditi Ltd., London, UK). The gap and width of the IDTs are specified by the SAW frequency, which, post-fabrication, was identified by measuring the reflection parameter S_{11} using a vector network analyzer (VNA; ZNB4, Rohde & Schwarz, Munich, Germany). To center the drop between the opposing IDT structures without requiring substrate patterning or surface preparation, we mounted a liquid dispenser (PV820, World Precision Instruments, Sarasota, USA) to dispense a drop of adjustable volume (maximum error of ±3%) at a position fixed between the IDTs. Between each experimental run, however, we clean the substrate surface by flushing with acetone, isopropyl alcohol and DI water, followed by drying using a nitrogen gun.

Initial results show that while it is possible to generate drop translation in opposite directions by driving these laterally segregated SAWs continually from both ends, this design alone was however insufficient to cause the drop to split. This is because the continuous application of SAW energy beyond the critical power required to sufficiently elongate and hence split the parent drop also causes undesirable partial jetting of the drop.[38] Additionally, symmetry breaking of the SAW irradiation into the drop as a consequence of the laterally-offset IDTs drives an internal rotational flow within the drop, as demonstrated previously.[29,37] While this internal rotational flow actually helps suppress the jetting to some extent, it also concurrently suppresses the elongation of both ends of the drop necessary for splitting. As such, it is necessary to confine the acoustic energy giving rise to both the jetting and rotation. Fortunately, the hydrodynamic time scales associated with both phenomena are sufficiently distinct such that we are able to split the energy input into the drop in the form of a sinusoidal SAW whose amplitude is modulated by a carrier waveform with two arbitrary-time-period components, as shown in Fig. 3. The first component, hereafter referred to as the rotational component, comprises a small amplitude excitation V_1 that while inadequate to produce jetting in the drop or to initiate translation by overcoming the contact line pinning, however allows the generation of a weak internal rotation over a period t_1—typically tens of milliseconds. This is followed by the second component, hereafter known as the splitting component—a sharp step increase in the excitation amplitude of the carrier signal V_2 over a period t_2. This splitting component provides the additional energy to overcome the rotational inertia to initiate translation in the horizontal direction and hence elongate the drop in opposite directions. If the elongation is sufficient at the point when the SAW irradiation is relaxed, capillary stresses cause the center of the elongated drop to neck such that the drop assumes a skewed dumbbell-like shape. Further drainage of the liquid from the neck under these forces then causes it to pinch into split droplets, which occurs over the Rayleigh time length scale.

We employ a 20 MHz amplitude modulated SAW corresponding to a wavelength, λ_{saw}, of approximately 200 μm (that this is smaller than the substrate thickness implies that bulk waves through the thickness of the substrate are weak compared to the SAW, and, moreover, the choice of 128° *Y–X* lithium niobate cut suppresses spurious bulk waves, including Lamb waves and plate modes; the attenuation length of the SAW on the substrate along the direction of its propagation is approximately 2 mm (ref. 39)) for the demonstration using a pair of coupled signal generators (SML01, Rohde & Schwarz, Munich, Germany; 33503A, Agilent, Santa Clara, CA, USA) together with an amplifier (ZHL-1-2W, Mini-Circuits,

Brooklyn, NY, USA); the SAW substrate vibration displacement u was determined using a Laser Doppler Vibrometer (LDV; MSA400, Polytec GmbH, Waldbronn, Germany) from which the power input into the drop can be derived:[40]

$$P = \frac{1}{2}\rho\omega^2 c_{SAW} d\int_0^{\infty}|u|^2 dx, \quad (1)$$

where ρ is the density of the drop with diameter d, and ω is the SAW frequency. As such, the relative energy inputs for the two components in the power delivery scheme can be determined by multiplying P by t_1 or t_2, respectively. Further, we confirm, through the use of the LDV, the absence of standing SAWs, which could form due to wave reflection at the edges of the device—these were eliminated in favour of two opposing travelling waves by placing absorbent material (α-gel, Taica Corporation, Tokyo, Japan) along the device's edges.

Top view drop splitting dynamics were imaged using a high speed video camera (Phantom Miro eX2, Vision Research, Wayne, NJ, USA) at 1000 frames s^{-1} mounted with a long-distance telescopic lens (K2-SC, Infinity, Boulder, CO, USA). The fluid velocity U was derived by the kymograph add-on within ImageJ software (National Institutes of Health, Behthesda, MD, USA), which monitors motion across multiple frames. Working fluids comprised deionized (DI) water, ethanol (Ethyl Alcohol 100%, Chem-Supply, Port Adelaide, SA, Australia) and glycerol solutions (99%, G5516, Sigma-Aldrich, Castle Hill, NSW, Australia); in some cases, surfactant (Tween-20; P2287, Sigma-Aldrich, Castle Hill, NSW, Australia) was added to alter the surface tension to study its effects.

3. Results and discussion

3.1 Splitting mechanism

Fig. 4 shows a typical image sequence showing the splitting of a parent sessile drop of DI water into two daughter droplets upon SAW excitation with the modulated energy input discussed above and shown in Fig. 3. It can be observed from the similar drop shape between the first two frames, corresponding to the beginning and endpoint of the rotational phase, that the input SAW energy E_R is only adequate to drive internal rotational flow within the drop and is not sufficient to overcome its surface free energy. Nevertheless, this initial flow aids in suppressing the undesirable effect of jetting that would arise when a sessile drop is directly commenced with sharp excitation of energy, similar to that of E_S (*i.e.*, if $t_1 = 0$).

We note that for a given initial parent drop size—characterized here by its radius R_M, the energy associated with the splitting component E_S appears to be independent of its rotational counterpart E_R beyond a critical time period t_c, commensurate with the hydrodynamic time scale associated with the jetting process. In other words, there needs to be sufficient time for the application of low amplitude rotational energy to suppress the drop jetting *via* compression (*i.e.*, $t_1 > t_c$). As long as this holds, the requisite energy input E_S for drop splitting is relatively independent of E_R; as such, E_S was observed to be independent of the initial energy state of the drop, but dependent on its initial dimension. This is conceivable for ideal drop splitting because E_S does not play a direct role in the actual splitting event; instead it only acts to stretch the drop beyond a critical elongation magnitude at which the capillary forces are unable to restore the drop to its original state when the SAW input energy is removed. This leads the capillary bridge spanning the two elongated ends of the drop to thin and eventually to pinch, as illustrated by the fourth frame in Fig. 4.

Given that E_R merely supplies the energy to drive internal circulation within the drop and does not play a direct role in its elongation or splitting, the difference in surface energies between the parent drop and the daughter droplets is then E_S, *i.e.*,

$$\gamma A_M + E_S = 2\gamma A_D, \quad (2)$$

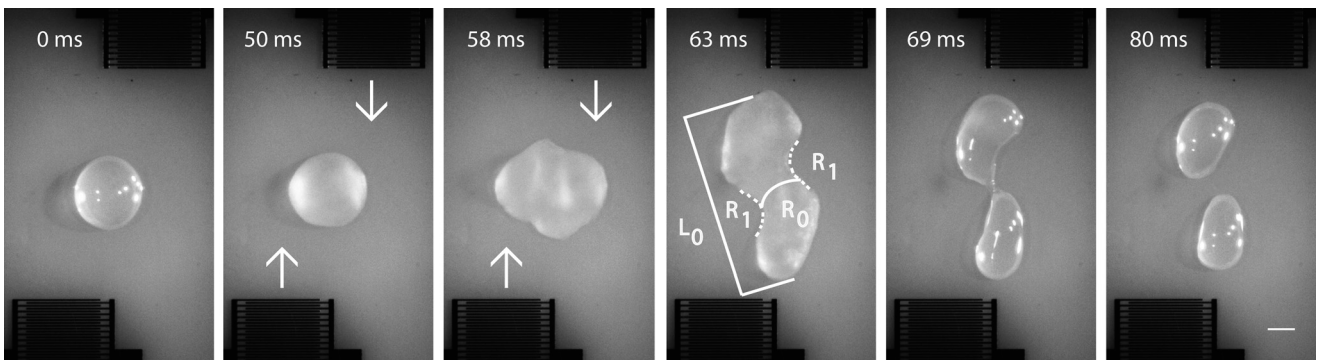

Fig. 4 Splitting of a 3 mL DI water drop using the modulated energy input described by Fig. 3, which comprises a longer low carrier amplitude rotational component to initiate internal rotational flow within the drop (V_1 = 0.1 mV, t_1 = 50 ms) followed by a shorter but more intense energy burst (V_2 = 1 V, t_2 = 13 ms) that causes the drop to elongate to form a neck that eventually pinches off over a period associated with the Rayleigh time scale $\mathscr{T}_R \sim (\rho R_0^3/\gamma)^{1/2} \sim 1$ ms to form two daughter droplets of equal volume. L_0 is the longitudinal stretch of the drop during the initial necking process when the SAW input is first relaxed, and R_0 and R_1 are its principal radii of curvature, respectively. The arrows depict the direction of the SAWs from the opposing IDTs, while the scale bar denotes a length of approximately 1 mm. The equilibrium contact angle of the post-split droplets are identical to that of the initial parent drop, which was found to be approximately 60°.

where γ is the surface tension, and, $A_M = 2\pi R_M^2$ and $A_D = 2\pi R_D^2$ are the surface areas of the parent drop and a daughter droplet, respectively, assuming the drop and droplets to be hemispherical. In the above, we have also assumed that the splitting leads to two daughter droplets of equal size—not unreasonable as will be observed below—and that external heating and viscous dissipation effects are negligible given the large Laplace number $Re^2/We \sim \rho R_0\gamma/\mu^2 \sim 10^5$, which is a measure of the relative contributions between capillary and viscous heating effects. $Re \equiv \rho U_L R_0/\mu$ and $We \equiv \rho U_L^2 R_0/\gamma$ are the Reynolds and Weber numbers, respectively, which will be discussed in more detail below; here, μ is the viscosity of the liquid, R_0 and L_0 the neck radius of curvature and the longitudinal stretch of the capillary bridge, respectively, at the instant when the SAW excitation is relaxed (as depicted by the fourth frame in Fig. 4), and U_L is the characteristic velocity scale associated with the SAW-induced inertial streaming flow that acts to elongate the drop towards the formation of the capillary bridge, obtained by measuring L_0 over the period of t_2 using the kymograph. Conserving the mass between the parent drop and the daughter droplets then requires $R_M = 2^{1/3}R_D$, which, in turn, leads to

$$E_S = 2\pi R_M^2\gamma(2^{2/3} - 1) \sim R_M^2. \quad (3)$$

This is not just qualitatively consistent with our observation of the dependence of E_S on the parent drop size; the predicted quadratic scaling can be seen in Fig. 5. To obtain the data for E_S in Fig. 5, the input power to the drop P associated with just the splitting phase was determined from eqn (1) using the surface displacement data obtained with the LDV and multiplied by t_2. To verify the values we obtain for E_S, we also subtracted E_R from the total energy E supplied to the drop. The former was obtained by assuming a rigid body for fluid circulation during the drop rotation phase such that $E_R \approx I\Omega^2$, wherein I is the moment of inertia for a rigid hemisphere and Ω is the angular speed of the fluid in the drop, measured by tracking 10 μm fluorescent particles seeded in the flow field. The latter, on the other hand, was calculated using eqn (1) with the LDV surface displacement data obtained over the entire duration associated with the rotational and splitting components. The average value of the y-intercept for the regression lines of 0.20 mJ deviates only slightly from the theoretical slope $2\pi\gamma(2^{2/3} - 1) = 0.27$ mJ.

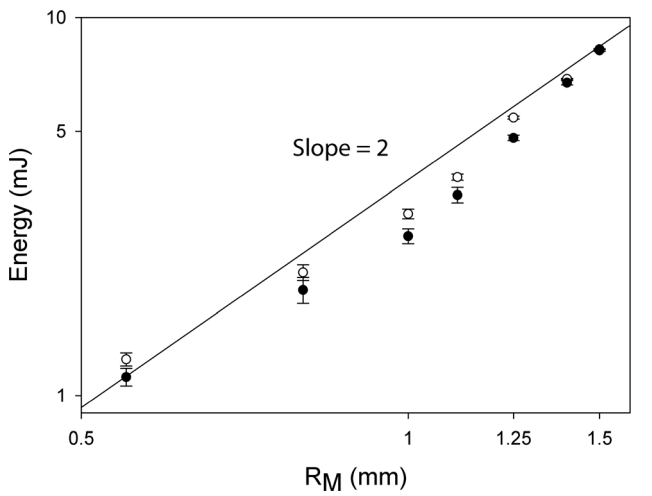

Fig. 5 Logarithmic dependence of E_S on the radius of the parent DI water drop R_M. E_S was measured directly using the LDV (open circles) as well as by subtracting the rotational energy E_R, obtained through particle image velocimetry measurements, from the total energy E, measured using the LDV (filled circles). The value of the y-intersect of the regression line is approximately 0.20 mJ.

3.2 Splitting regimes

The phase map in Fig. 6A illustrates how the power associated with the splitting energy component $E_S = P_S t_2$ leads to different splitting regimes for parent DI water drop volumes between 0.5 and 6 μL. As expected, splitting does not occur until sufficient energy is applied, defined by the boundary between Regimes I and II. The collapse of the data seen in Fig. 6B by rescaling the energy with respect to the Weber number We (which captures the relative contributions between the inertial stress imposed on the parent drop through the internal fluid streaming generated within it to elongate the drop and the capillary stress embodied by the drop's surface energy which acts to retard the elongation) and a dimensionless aspect ratio $\Lambda_0 \equiv L_0/R_0$, then reveals that drop breakup occurs over a constant critical Weber number of approximately 0.64. Below this critical value, the inertia from the SAW induced streaming is inadequate to produce a sufficient stretch Λ_0, and hence a sufficiently large enough capillary bridge pressure $\gamma(1/R_1 - 1/R_0)$ to effectively drive the drainage of the liquid within the bridge towards both ends of the elongated drop such that it pinches; R_0 and R_1 being the principal radii of curvature of the neck at the instant when the SAW excitation is relaxed. Instead, the negative capillary bridge pressure characterized by $R_1 < R_0$ results in the retraction of the liquid from both longitudinal ends of the drop back into the capillary bridge, expanding R_0 outward axially until the elongated drop contracts to its original R_M drop footprint—its initial lowest surface energy state and shape. The constant critical We value also suggests then that it is the energy (*i.e.*, the area under the curve in Fig. 6A) rather than the power that is the important parameter in determining the splitting behavior of the drop: the same result is expected for higher powers and shorter times t_2, or *vice versa*, if the energy and the physical properties of the liquid remain constant, at least for the conditions we examine.

Above the critical Weber number (regimes II–IV), the sufficiently elongated drop with $R_1 < R_0$ results in a positive capillary bridge pressure that dictates drainage of the liquid from the high pressure capillary bridge into the longitudinal ends of the drop. As a consequence, R_0 decreases as the pressure within the capillary bridge increases, resulting in the drop assuming a dumbbell-like shape, until capillary instabilities

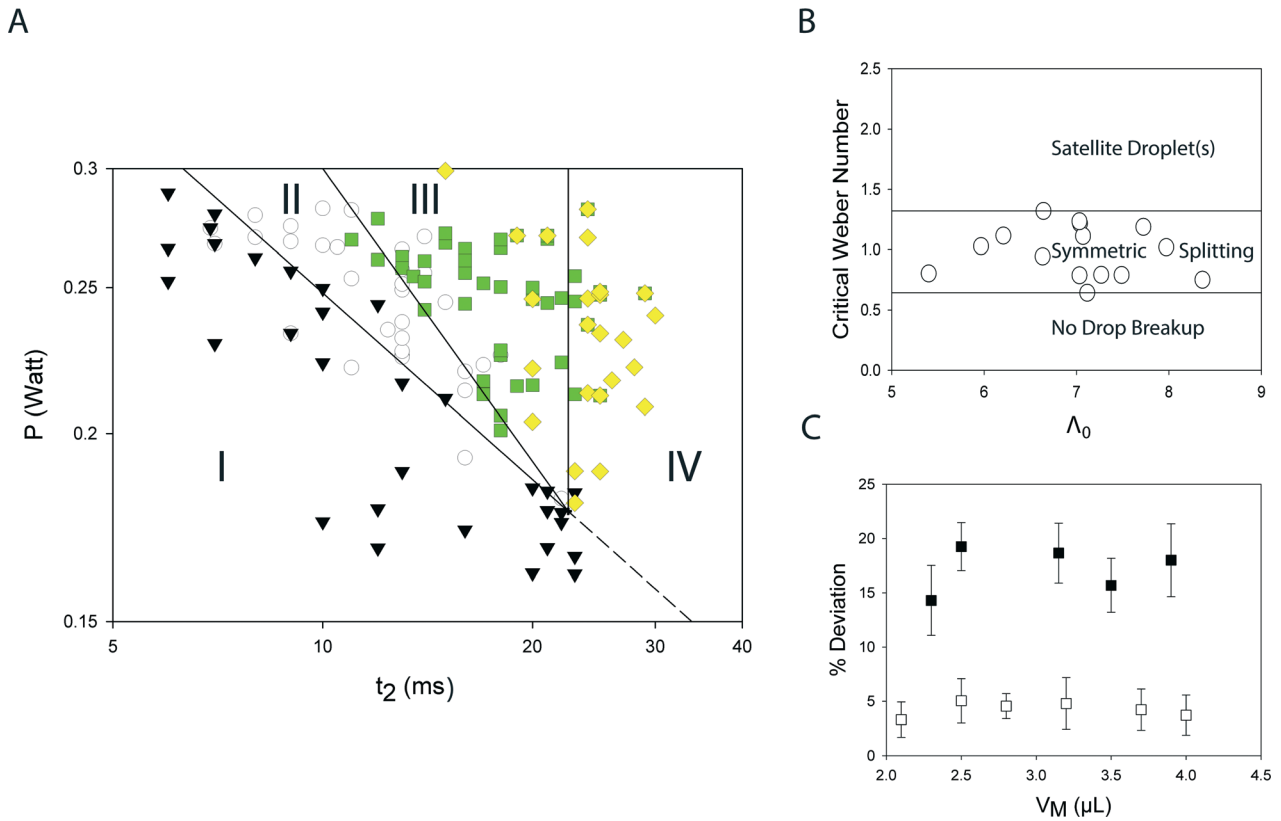

Fig. 6 (A) Phase map showing the different drop splitting behaviors observed for DI water droplets across a range of volumes (0.5–6 mL) as a function of the input power P to the device and the total time over which the SAW energy associated with the splitting component in Fig. 3 is applied t_2. Regime I (black inverted triangles): no splitting (insufficient input power and hence elongation of the parent drop); regime II (white circles): ideal splitting into two daughter droplets; regime III (green squares): non-ideal splitting in which one or more satellite droplets are produced in addition to the two daughter droplets; regime IV (yellow diamonds): oversupply of input power, resulting in droplet translation, reflection and coalescence, possibly followed by a resplitting event. (B) Collapse of the data in Regime II upon rescaling with the Weber number $We \equiv \rho U_L^2 R_0/\gamma$ and a dimensionless aspect ratio $\Lambda_0 \equiv L_0/R_0$, depicting that splitting (*i.e.*, the boundary between regimes I and II) occurs at a constant value of the critical Weber number. Sample size: n = 115. (C) Difference in the volumes of the symmetrical daughter droplets produced during the splitting events in regime II for the range of parent drop volumes between 2 and 4.5 μL, characterized as a percentage of the total volume, for the case in which the splitting is driven with (open squares) and without (filled squares) the amplitude–modulated carrier waveform. Sample size: n = 115.

ultimately drive its collapse. The point of failure of the capillary bridge determines the final outcome of the splitting process and, in particular, is determined by the aspect ratio of the drop, *i.e.*, Λ_0, and consequently E_S. At moderate energies such that the Weber number is just above the critical value (regime II), a small value of Λ_0 ensues such that the relatively short capillary bridge leads to complete drainage of the liquid to the protrusions at both ends, thus resulting in an ideal split of the parent drop into two daughter droplets. An increase in the energy, for example by increasing t_2 at constant input SAW power (regime III), however, causes further elongation of the parent drop, L_0, and hence the length of the capillary bridge to a point at which it becomes susceptible to instabilities that resemble Rayleigh–Plateau instabilities in the thinning of axisymmetric liquid bridges.[41,42] As a consequence of these instabilities, the liquid bridge pinches at multiple points associated with the wavelength of the instability, thus resulting in the formation of satellite droplets in between the two daughter droplets. Λ_0 increases with E_S and hence a greater number of satellite droplets are produced as the energy supplied in the splitting component is increased, as seen in Fig. 6A. The size of the satellite droplets generated, on the other hand, depends on the volume of the liquid bridge, in particular the lateral dimension R_0. At yet higher powers (regime IV), the large energy input causes the split droplets to translate by Eckart streaming to the opposing IDT followed by their subsequent reflection, which may lead to recoalescence and their tendency to resplit.

Whilst this could constitute one way to drive the merging of droplets, a better and more reproducible method for merging droplets is to employ focused IDTs at both ends to translate two droplets toward each other such that their collision with sufficient energy results in their coalescence and hence merger at the focal point of the SAWs,[29] as shown in Fig. 7. This ability to merge or simply align a drop at the focal point of the SAW can be quite useful for positioning the initial parent drop such that it is exactly centered between the two opposing IDTs, which is necessary for ideal splitting and which becomes increasingly difficult for parent drops below 0.5 μL.

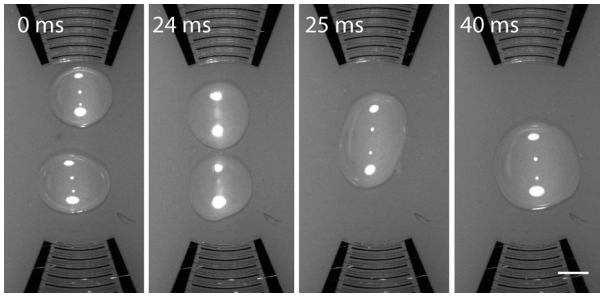

Fig. 7 Droplet coalescence using a pair of focused IDTs with a resonance frequency of 30.3 MHz to drive the translation of the droplets toward the focal point of the SAWs. Here, a ramp-up in the input power to 0.1 W is employed. After their coalescence, which occurs in the 1 ms between the second and third frames, additional SAW energy is applied to center the drop at the focal point of the IDTs. The scale bar denotes a length of approximately 1.5 mm.

Table 1 Physical properties of the test liquids used

		μ (N s m^{-2})	γ (N m^{-1})	ρ (kg m^{-3})	t_2 (ms)
DI water	21 °C	0.0010	0.0728	1000	13.0
	40 °C	0.0065	0.0696	992.2	10.0
Ethanol	3.3%	0.0013	0.0562	987.1	10.0
	7.2%	0.0016	0.0443	974.1	8.6
	11.2%	0.0020	0.0361	959.4	7.8
	17.1%	0.0023	0.0308	942.9	7.3
	23.6%	0.0024	0.0278	924.3	7.1
	31.6%	0.0024	0.0266	903.6	7.0
Glycerol	10%	0.0012	0.0720	1030.0	15.0
	20%	0.0016	0.0713	1060.9	25.0
	30%	0.0022	0.0706	1090.4	30.0
	40%	0.0033	0.07058	1118.4	45.0
20% Glycerol–Tween 20 (0.075%)		0.0058	0.0411	1055.9	20.0

To ascertain the accuracy, reliability, and reproducibility of the proposed SAW splitting technique, we compare the volumes of the two daughter droplets that are produced over a large number of sample runs of $n = 115$, carefully minimizing losses due to evaporation although such effects are typically negligible over the short experiment times, especially for droplet volumes above 1 μL.[43] Fig. 6C shows the possibility of precise and reproducible splitting with the present amplitude-modulation scheme: across the range of parent drop volumes between 2 to 4 μL, we obtain average deviations between the volumes of the split droplets of around 4.3%, with a single deviation not exceeding 10%. This is comparable to electrowetting, in which a maximum deviation of 7% was obtained for parent drop volumes between 1.2 and 3.2 μL.[44] In the absence of amplitude-modulation of the carrier waveform, we however see in Fig. 6C the large discrepancies and variation in the sizes of the daughter droplets that are produced, therefore underlining the importance of the role of the carrier signal modulation, particularly in suppressing jetting effects and hence the consequent loss of liquid.

3.3 Effect of physical properties

Having explored the splitting dynamics for DI water drops, we now briefly turn to an investigation of the effect of the liquid's physical properties on the splitting process. To allow for variations in both viscosity and surface tension, we employed ethanol and glycerol solutions of varying concentration. In addition, we also heated the DI water as well as added surfactant to a glycerol solution. The various liquids used and their physical properties are summarized in Table 1. In particular, the larger the surface tension, the larger the surface free energy and hence the restoring capillary stress that is required to overcome the elongation and hence pinch the drop. On the other hand, the more viscous the fluid, the greater the viscous retardation of the fluid which opposes its flow both during the elongation of the parent drop—thus opposing the inertial energy provided by E_S to attain a sufficient stretch Λ_0—as well as during the drainage of the capillary bridge into the protrusions at both ends.

Since the Weber number defined above does not account for viscous effects, the threshold energy above which the splitting event occurs can no longer be adequately characterized by the critical Weber number in Fig. 8A. Instead, the capillary bridge thinning dynamics must be accounted for by coupling the Weber number with the Reynolds number,[45] which captures the relative contributions between the inertial and viscous stresses associated with the flow in the capillary bridge. Concomitantly, in Fig. 8B we have recast our data into such a parameter—a critical Ohnesorge number $\mathrm{Oh} \equiv \mathrm{We}^{1/2}/\mathrm{Re} \equiv \mu/(\rho\gamma R_0)^{1/2}$, from which we note the onset of splitting occurs below a critical value of approximately 0.01 across the liquids tested.

The Ohnesorge number can also be defined as the ratio between the inertial (Rayleigh) and viscous time scales associated with the thinning dynamics of the capillary bridge, *i.e.*, $\mathrm{Oh} \equiv \mathscr{T}_v/\mathscr{T}_R$, wherein $\mathscr{T}_R \sim (\rho R_0{}^3/\gamma)^{1/2} \sim 10^{-3}$ s and $\mathscr{T}_v \sim \mu R_0/\gamma \sim 10^{-5}$ s are the Rayleigh and viscous time scales, respectively; we observe that the former is consistent with the 1 ms order duration over which the capillary bridge pinches in Fig. 4. Given that $\mathrm{Oh} \ll 1$ or $\mathscr{T}_v \ll \mathscr{T}_R$, we note that the thinning of the capillary bridge is essentially inertially-dominated, *i.e.*, the liquids behave as inviscid fluids given their low viscosities, reminiscent of those found in the stretching of liquid bridges, *e.g.*, using a capillary breakup extensional rheometer (CABER),[41] as well as those using SAW jets.[42]

The above consistently reinforces our previous assertion in section 3.1 that ideal drop splitting is dependent only on the capillary thinning dynamics that is initiated upon the removal of the input energy to the drop, and independent of E_S and the elongation of the drop, provided that the drop is sufficiently stretched beyond the point at which it can be restored to its original shape by capillary forces. This claim is further supported, in fact, by replacing the characteristic velocity U_L associated with the elongation flow induced by the energy component E_S in the Weber number with the characteristic velocity associated with the necking $U_n \equiv R_0/\mathscr{T}_R$

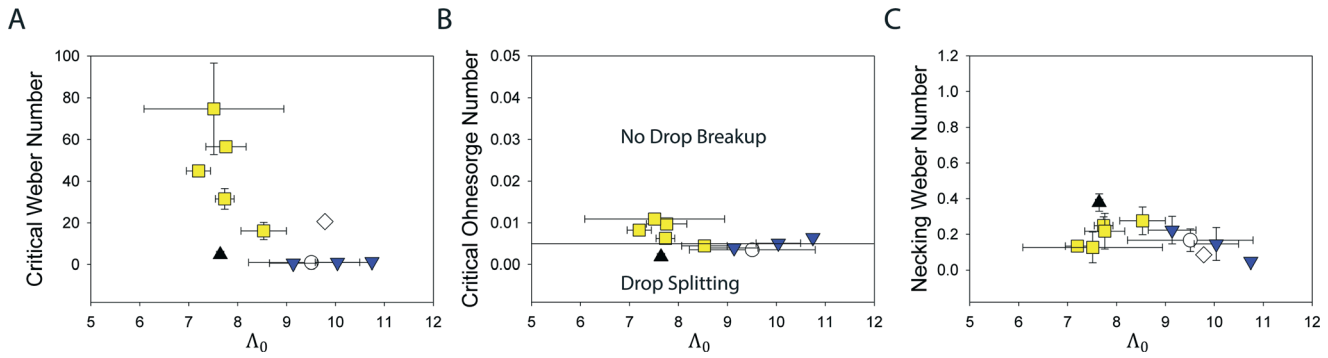

Fig. 8 (A) Critical values of the Weber number $We \equiv \rho U_L^2 R_0/\gamma$ at the onset of splitting for a 3 mL drop as a function of a dimensionless aspect ratio $\Lambda_0 \equiv L_0/R_0$ for the liquids tabulated in Table 1 (white circles: DI water at 21 °C; black triangles: DI water at 40 °C; blue inverted triangles: glycerol solutions of different concentrations; yellow squares: ethanol solutions of different concentrations; white diamonds: glycerol–Tween 20 solution). Sample size: n = 130. Collapse of this data can be seen in (B) by rescaling with a critical Ohnesorge number $Oh \equiv \mu/(\rho\gamma R_0)^{1/2}$ or (C) by rescaling with a critical necking Weber number $We_n \equiv \rho U_n^2 R_0/\gamma$, wherein $U_n \equiv R_0/\mathcal{T}_R$ is the characteristic necking velocity.

(measured using a kymograph across the contracting capillary bridge). Doing so leads to the collapse in the data in Fig. 8A to a constant value of the critical necking Weber number $We_n \equiv \rho U_n^2 R_0/\gamma$, as seen in Fig. 8C.

4. Asymmetric splitting

Beyond splitting of a parent drop into two symmetric daughter droplets (Fig. 4 and 6), it is also possible to controllably split the drop asymmetrically by supplying the IDTs with different input powers. Although the opposing 20 MHz IDT pairs were ostensibly identical, it was necessary to compensate for the sensitivity of each IDT's impedance to variations in their finger and gap widths. These were individually measured by isolating the opposing IDT with the use of α-gel, which then provided values of the IDT's S_{11} frequency spectra. Once calibrated, we were able to drive known ratios of input energy across the device from the two IDTs. Weighting the input power in favour of one IDT over the other leads to a longitudinal shift in the location at which the capillary bridge of the elongated drop forms away from the center, resulting in a corresponding spatial shift in the location where the necking occurs. This then results in an asymmetric partitioning of the drainage of the capillary bridge, therefore producing daughter droplets of different sizes.

Example daughter droplets with 1 : 2 and 1 : 5 volume proportions generated through such an asymmetric splitting scheme are shown in Fig. 9A and B. Fig. 9C in fact shows a linear dependence of the ratio of the volumes of the smaller daughter droplet to that of the parent drop V_{D1}/V_M on the ratio of the IDT impedances Z_1/Z_2 for a 3 μL DI water drop at room temperature, confirmed by a similar trend in the ratio of the SAW powers from each IDT P_1/P_2 (as measured using the LDV), shown in the same plot. It can also be seen from Fig. 9C that the greater the droplet asymmetry, *i.e.*, the further the value of V_{D1}/V_M from 0.5, the larger the difference in the input energy to the IDTs that is required, *i.e.*, P_1/P_2 increasingly deviates from a value of 1 where both the input energy to the IDTs are identical. Asymmetric splitting with daughter droplet volume proportions $V_{D1} : V_{D2}$ of 1 : 5, 1 : 4, 1 : 3, 1 : 2, 2 : 3, and 4 : 5 (corresponding to V_{D1}/V_M values of 0.166, 0.2, 0.25, 0.333, 0.4, and 0.44, respectively) were successfully conducted in this manner on a single device, without necessitating different electrode configurations for each variation in the droplet volume proportions as is required in electrowetting.

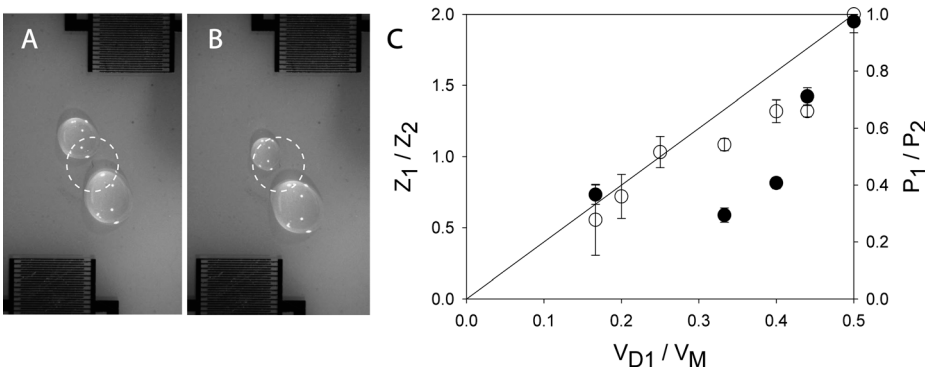

Fig. 9 Asymmetric splitting of a DI water drop into droplets with (A) 1 : 2 and (B) 1 : 5 volume proportions; dotted circles represent the initial position of the parent drop prior to splitting. (C) Dependence of the volume ratio between the smaller daughter droplet and the parent drop it was split from $V_{D1} = V_M$ on the difference between the IDT impedances (open circles; left axis) and input power (filled circles; right axis).

5. Conclusions

Here, we have reported a comparable and alternative platform to electrowetting schemes for carrying out drop manipulations such as merging and splitting on a planar microfluidic device using modulated SAWs generated from both ends of the device using a pair of laterally offset transducers. In particular, a two-component carrier waveform for the 20 MHz SAW is employed. The initial component consists of a small modulation amplitude over longer times compared to the hydrodynamic time scale associated with drop jetting—typically tens of ms—that initiates rotational streaming within the parent drop while the subsequent component consists of a sharp burst—typically 10 ms—with a large modulation amplitude such that the inertial stresses arising from the streaming within the drop causes it to elongate. The final splitting of the drop however requires the energy associated with the second component, which scales quadratically with the dimension of the parent drop, to lie above a threshold energy level, which can be described by a critical Ohnesorge number, such that capillary stresses lead to the formation of a liquid bridge between the two ends of the elongated drop, which upon relaxation of the SAW excitation, drains and hence pinches to form a split droplet pair. Above the critical Ohnesorge number, however, there is insufficient inertial stress to adequately elongate the drop such that the capillary pressure of the liquid bridge is insufficient to cause it to drain, and the drop simply retracts. We show that drops across a volume range between 0.5 and 6 μL can be symmetrically split to reproducibly produce droplets of equal size with around 4.3% deviation, on average, and not exceeding 10%. This favourably compares with the 7% upper limit in the splitting efficiency of electrowetting schemes. Unlike electrowetting, however, the size of the drops are not dependent on the electrode dimension and hence drops of different volumes can be manipulated on the same device without having to resort to the fabrication of separate devices with different electrode configurations. Further, the splitting can be tuned by applying different input powers or by varying the excitation periods for both energy components. Indeed, we have demonstrated the possibility for asymmetric splitting to controllably and reproducibly produce droplets with different sizes simply by applying different energy levels to both IDTs.

Acknowledgements

We are grateful to Amgad Rezk, Amarin McDonnell, and Gopesh Tilvawala for helpful discussions on device fabrication and the capillary thinning dynamics. LYY is grateful for a Future Fellowship (FT130100672) from the Australian Research Council (ARC), who also funded part of the work through Discovery Project grant DP140100805.

References

1 J. Zeng and T. Korsmeyer, *Lab Chip*, 2004, **4**, 265–277.
2 K. Choi, A. H. Ng, R. Fobel and A. R. Wheeler, *Annu. Rev. Anal. Chem.*, 2012, **5**, 413–440.
3 A. R. Wheeler, *Science*, 2008, **322**, 539–540.
4 J.-Y. Yoon and R. L. Garrell, *Anal. Chem.*, 2003, **75**, 5097–5102.
5 M. G. Pollack, V. K. Pamula, V. Srinivasan and A. E. Eckhardt, *Expert Rev. Mol. Diagn.*, 2011, **11**, 393–407.
6 L. Y. Yeo, H.-C. Chang, P. P. Y. Chan and J. R. Friend, *Small*, 2011, **7**, 12–48.
7 B. Berge and J. Peseux, *Eur. Phys. J. E: Soft Matter Biol. Phys.*, 2000, **3**, 159–163.
8 R. A. Hayes and B. Feenstra, *Nature*, 2003, **425**, 383–385.
9 S. Haeberle and R. Zengerle, *Lab Chip*, 2007, **7**, 1094–1110.
10 S. K. Cho, H. Moon and C.-J. Kim, *J. Microelectromech. Syst.*, 2003, **12**, 70–80.
11 H. Mertaniemi, V. Jokinen, L. Sainiemi, S. Franssila, A. Marmur, O. Ikkala and R. H. Ras, *Adv. Mater.*, 2011, **23**, 2911–2914.
12 F. Mugele and J.-C. Baret, *J. Phys.: Condens. Matter*, 2005, **17**, R705.
13 L. Yeo, R. Craster and O. Matar, *J. Colloid Interface Sci.*, 2007, **306**, 368–378.
14 L. Y. Yeo and H.-C. Chang, *Phys. Rev. E: Stat., Nonlinear, Soft Matter Phys.*, 2006, **73**, 011605.
15 K. H. Kang, *Langmuir*, 2002, **18**, 10318–10322.
16 L. Y. Yeo and H.-C. Chang, *Mod. Phys. Lett. B*, 2005, **19**, 549–569.
17 M. G. Pollack, R. B. Fair and A. D. Shenderov, *Appl. Phys. Lett.*, 2000, **77**, 1725–1726.
18 R. B. Fair, *Microfluid. Nanofluid.*, 2007, **3**, 245–281.
19 X. Ding, P. Li, S.-C. S. Lin, Z. S. Stratton, N. Nama, F. Guo, D. Slotcavage, X. Mao, J. Shi and F. Costanzo, *et al.*, *Lab Chip*, 2013, **13**, 3626–3649.
20 L. Y. Yeo and J. R. Friend, *Annu. Rev. Fluid Mech.*, 2014, **46**, 379–406.
21 D. Beyssen, L. Le Brizoual, O. Elmazria and P. Alnot, *Sens. Actuators, B*, 2006, **118**, 380–385.
22 A. Renaudin, P. Tabourier, V. Zhang, J. Camart and C. Druon, *Sens. Actuators, B*, 2006, **113**, 389–397.
23 M. K. Tan, J. R. Friend and L. Y. Yeo, *Lab Chip*, 2007, **7**, 618–625.
24 X. Du, Y. Fu, J. Luo, A. Flewitt and W. Milne, *J. Appl. Phys.*, 2009, **105**, 024508.
25 P. Brunet, M. Baudoin, O. B. Matar and F. Zoueshtiagh, *Phys. Rev. E: Stat., Nonlinear, Soft Matter Phys.*, 2010, **81**, 036315.
26 Y. Ai and B. L. Marrone, *Microfluid. Nanofluid.*, 2012, **13**, 715–722.
27 M. Travagliati, G. De Simoni, C. M. Lazzarini, V. Piazza, F. Beltram and M. Cecchini, *Lab Chip*, 2012, **12**, 2621–2624.
28 A.-L. Zhang, Z.-Q. Wu and X.-H. Xia, *Talanta*, 2011, **84**, 293–297.
29 R. Shilton, M. K. Tan, L. Y. Yeo and J. R. Friend, *J. Appl. Phys.*, 2008, **104**, 014910.
30 T. Frommelt, M. Kostur, M. Wenzel-Schäfer, P. Talkner, P. Hänggi and A. Wixforth, *Phys. Rev. Lett.*, 2008, **100**, 034502.
31 R. J. Shilton, L. Y. Yeo and J. R. Friend, *Sens. Actuators, B*, 2011, **160**, 1565–1572.

32 A. Wixforth, C. Strobl, C. Gauer, A. Toegl, J. Scriba and Z. V. Guttenberg, *Anal. Bioanal. Chem.*, 2004, **379**, 982–991.

33 Z. Guttenberg, H. Müller, H. Habermüller, A. Geisbauer, J. Pipper, J. Felbel, M. Kielpinski, J. Scriba and A. Wixforth, *Lab Chip*, 2005, **5**, 308–317.

34 A. Zhang, Y. Zha and X. Fu, *AIP Adv.*, 2013, **3**, 072119.

35 Y. Bourquin, R. Wilson, Y. Zhang, J. Reboud and J. M. Cooper, *Adv. Mater.*, 2011, **23**, 1458–1462.

36 Y. Li, Y. Q. Fu, S. D. Brodie, M. Alghane and A. J. Walton, *Biomicrofluidics*, 2012, **6**, 012812.

37 H. Li, J. R. Friend and L. Y. Yeo, *Biomed. Microdevices*, 2007, **9**, 647–656.

38 M. K. Tan, J. R. Friend and L. Y. Yeo, *Phys. Rev. Lett.*, 2009, **103**, 024501.

39 M. B. Dentry, L. Y. Yeo and J. R. Friend, *Phys. Rev. E: Stat., Nonlinear, Soft Matter Phys.*, 2014, **89**, 013203.

40 D. Royer and E. Dieulesaint, *Elastic Waves in Solids II: Generation, Acousto-Optic Interaction, Applications*, Springer, 2000, vol. 2.

41 L. E. Rodd, T. P. Scott, J. J. Cooper-White and G. H. McKinley, *Appl. Rheol.*, 2005, **15**, 12–27.

42 P. Bhattacharjee, A. McDonnell, R. Prabhakar, L. Yeo and J. Friend, *New J. Phys.*, 2011, **13**, 023005.

43 C. G. Cooney, C.-Y. Chen, M. R. Emerling, A. Nadim and J. D. Sterling, *Microfluid. Nanofluid.*, 2006, **2**, 435–446.

44 R. Fair, V. Srinivasan, H. Ren, P. Paik, V. Pamula and M. Pollack, *Proceedings of the IEEE International Electron Devices Meeting IEDM'03*, 2003, pp. 32–35.

45 J. Eggers, *Rev. Mod. Phys.*, 1997, **69**, 865–929.